

Reprinted from the Journal of The American Ceramic Society, Vol. 60, No. 9-10 September-October, 1977.  
Copyright 1977 by The American Ceramic Society

# Strength Degradation of Glass Resulting from Impact with Spheres

S. M. WIEDERHORN\*

Institute for Materials Research, National Bureau of Standards, Washington, D.C. 20234

B. R. LAWN

Department of Applied Physics, School of Physics, University of New South Wales, Kensington, New South Wales 2033, Australia

The nature and extent of degradation incurred by glass surfaces impacted with spheres of steel and tungsten carbide were studied. The residual strength after impact depends on the velocity, radius, and density of the projectile; on the toughness and (indirectly) the hardness of the target; and, to a lesser degree, on the preexisting mechanical condition of the surface. The damage morphology involves modification of the basic Hertzian cone crack pattern by median (radial) cracks and crushed glass at the impact site. The essential features of the degradation may be predicted by a theoretical analysis of residual strength as a function of impact velocity as derived from indentation fracture mechanics. This study accounts, in particular, for a threshold velocity for significant strength loss,

above which further strength decrease is relatively slight. Small, but significant, discrepancies between observed and predicted degradation characteristics are attributed to the departure from ideal Hertzian fracture geometry and to the dynamic nature of the contact. However, it is suggested that quasi-statically based theory may be used for estimating the strength of structural ceramics in small-particle impact situations.

---

Received November 20, 1976; revised copy received March 16, 1977.  
Supported by the U.S. Office of Naval Research and the Australian Research Grants Committee.  
\*Member, the American Ceramic Society.

## I. Introduction

**B**ECAUSE they lack ductility, glasses and other ceramic materials are highly susceptible to microfracture damage from impact with hard particles. Although the damage may be barely detectable by visual inspection, it can result in a drastic reduction in strength; the slightest contact of a single particle with a pristine glass surface can reduce the strength by orders of magnitude,<sup>1</sup> a fact well-known to those involved in the fabrication of fiber glass materials. Ordinary ceramics containing an abundance of preexisting flaws show a less pronounced, but not insignificant, effect. Ashford,<sup>2</sup> for example, recorded a fivefold reduction in the strength of silicon carbide rods impacted with small steel spheres. It is apparent that the mechanical damage associated with particle impact events can be severe and needs to be considered when ceramics are designed for structural applications.

In two previous papers,<sup>3,4</sup> the strength degradation of glass surfaces was studied for essentially static indenter loading. Indenters were classified into two types: "blunt" indenters (spheres),<sup>3</sup> characterized by an elastic contact, resulting in the formation of the classical Hertzian type of cone crack; "sharp" indenters (cones, pyramids),<sup>4</sup> with a plastic contact, resulting in the formation of median and lateral cracks. These indentation configurations conveniently bracket those observed in real contact situations. Particles encountered in practice (e.g. dust particles) will tend to be blunt if well worn, sharp if freshly crushed.

The present study extends the static analysis to impact with blunt indenters. We promote the philosophy that strength degradation characteristics should be predictable from simple fracture parameters as measured in standard indentation tests.<sup>5</sup> Thus, the previously cited glass indentation data are used to evaluate appropriate impact parameters in the present analysis. A key point in the formulation is the application of the Hertzian contact equations to derive a relation between impact velocity and load. In conjunction with basic strength and indentation relations for equilibrium cracks,<sup>3</sup> this formulation leads to a strength/velocity degradation characteristic for a given projectile/target system. This quasi-static approach was first applied to the degradation problem by Evans<sup>6</sup>; our analysis is directed specifically to providing simplified working expressions in which the controlling variables are readily identified and investigated. Essential predictions of the theory are confirmed by impact experiments on glass slabs using small spherical projectiles (<1 mm radius) at velocities up to 300 m s<sup>-1</sup>.

## II. Prediction of Impact-Induced Strength Degradation

In a contact situation, strength degradation is a result of damage caused by highly concentrated stresses below the indenting particle. In brittle solids such as silicate glass, where stress relief by deformation processes such as plasticity and densification is limited, the loss of strength is directly attributable to the formation of indentation cracks. Expressions for the size of the cracks as a function of contact load are obtainable from indentation fracture mechanics.<sup>5</sup> When the Hertzian theory of elastic contact<sup>7</sup> is used to determine a relation for the impact load delivered by a sphere, the crack size may then be related to particle velocity; the degradation may then be predicted from standard strength equations.

### (1) Impulsive Load Delivered by Impacting Sphere

First, we estimate the maximum load,  $P_m$ , delivered to a flat target surface by a sphere of velocity  $v$ . Assuming that the impact process occurs slowly compared to the velocity of stress waves in the contacting materials and that the onset of any deformation or fracture absorbs a negligible amount of energy, the Hertzian solutions of the equilibrium equations of elastic contact yield<sup>7</sup>

$$P_m = [(125\pi^3/48)^{1/5} (E/k)^{2/5} \rho^{3/5} r^{2/5}] v^{6/5} \quad (1)$$

Here  $r$  is the radius and  $\rho$  the density of the sphere, and  $k = (9/16)[(1-\nu^2) + (1-\nu'^2)E/E']$  is a dimensionless constant with  $\nu$  Poisson's ratio and  $E$  Young's modulus (the primes refer to the indenter material). We might expect this quasi-statically based relation to remain a reasonable approximation over a large part of the subsonic impact velocity regime, if the damage is not too great.<sup>8</sup>

### (2) Indentation Fracture Relations

As the load delivered by the impacting particle increases rapidly to a maximum, preexisting flaws experience a correspondingly rapid increase in tensile stress. A sufficiently high stress will cause a favorably located surface flaw to run around the contact circle in a ring-like fashion and then flare suddenly downward into a full cone crack. Static indentation studies have shown that the cone crack does not form until after a critical load is exceeded. Thus, in the impact case, we must expect the strength degradation to be insignificant below some threshold velocity. When the target surface contains an abundance of large potential starting flaws, application of the Griffith energy-balance condition for equilibrium cracks gives the critical load<sup>5,8,9</sup>

$$P_c = 2\Gamma r k / \phi^* = K_c r k / E \phi_1^* \quad (2)$$

where the fracture-surface energy  $\Gamma$  and critical stress-intensity factor  $K_c = [2\Gamma E / (1-\nu^2)]^{1/2}$  are interchangeable fracture mechanics parameters, and  $\phi^* = \phi^*(\nu)$  and  $\phi_1^* = \phi_1^*(\nu) = \phi^*(\nu)(1-\nu^2)$  are dimensionless material constants whose values are usually obtained empirically.<sup>5</sup> This relation, known as Auerbach's law,<sup>9</sup> actually breaks down for small flaws or large spheres,<sup>8</sup> but, since it represents a "worst-case" situation, it will serve as a conservative basis for estimating the critical conditions for the onset of strength loss.<sup>3</sup> The appropriate threshold velocity is therefore obtained by putting  $P_m = P_c$  in Eqs. (1) and (2):

$$v_c = (48/125\pi^3)^{1/6} (k/E)^{7/6} K_c^{5/3} / \rho^{1/2} r^{5/6} \phi_1^{5/6} \quad (3)$$

When a cone crack is formed it continues to grow, in a stable manner, as the impulsive load exceeds the threshold. Using a dimensional analysis in conjunction with the Griffith energy-balance concept, Roesler<sup>10</sup> derived a simple equilibrium relation between indentation load and crack size for a true cone:

$$P/R^{3/2} = (2\Gamma E / \kappa_R)^{1/2} = \beta_R K_c \quad (P > P_c, R \gg R_0) \quad (4)$$

where  $R$  is the base radius of the cone (subscript zero referring to surface trace) and  $\kappa_R = \kappa_R(\nu)$  and  $\beta_R$  are constants which are usually determined empirically.<sup>5</sup> The crack size may now be expressed in terms of the impact velocity by putting  $P_m = P$  in Eqs. (1) and (4):

$$R = [(125\pi^3/48)^{2/15} (E/k)^{4/15} \rho^{2/15} r^{4/3} / \beta_R^{2/3} K_c^{2/3}] v^{4/5} \quad (v > v_c) \quad (5)$$

### (3) Strength Equations

We may now obtain explicit relations for the strength degradation in terms of the impact velocity. We write the standard expression for the tensile strength

$$\sigma = [2\Gamma E / \pi(1-\nu^2)c_f]^{1/2} = K_c / (\pi c_f)^{1/2} \quad (6)$$

where  $c_f$  is the effective length of the dominant flaw. The source of this flaw in an impacted specimen will depend on the threshold velocity condition (Eq. (3)) for cone crack formation. Below  $v_c$  the strength is determined by the preexisting flaw distribution in the glass surface: for example, in a surface subjected to controlled abrasion treatment, we would expect the effective length of the dominant flaw to remain independent of impact velocity, at a value  $c_f = c_f^0$  characteristic of the abrasion damage. Above  $v_c$ , the strength decreases precipitously and is determined entirely by the size of the fully developed cone crack: then at  $R \gg R_0$  the effective flaw length assumes the form  $c_f = R\Omega$ , where  $\Omega = \Omega(\alpha)$  is a dimensionless function of the cone angle  $\alpha$  (angle between cone and specimen surface) evaluated elsewhere.<sup>3</sup>

Thus, from Eqs. (5) and (6), we obtain the following expressions for the strength, which, in conjunction with the threshold Eq. (3), constitute the degradation characteristics:

$$\sigma = K_c / (\pi c_f^0)^{1/2} \quad (v < v_c) \quad (7a)$$

$$\sigma = [(48/125\pi^{10.5})^{1/15} (k/E)^{2/15} \beta_R^{1/3} K_c^{4/3} / \Omega^{1/2} \rho^{1/5} r^{2/3}] v^{-2/5} \quad (v > v_c) \quad (7b)$$

## III. Impact Degradation Tests

### (1) Impact Test Procedure

For these studies we used an air gun to accelerate the spherical projectiles, and an electromagnetic velocity analyzer. The air gun

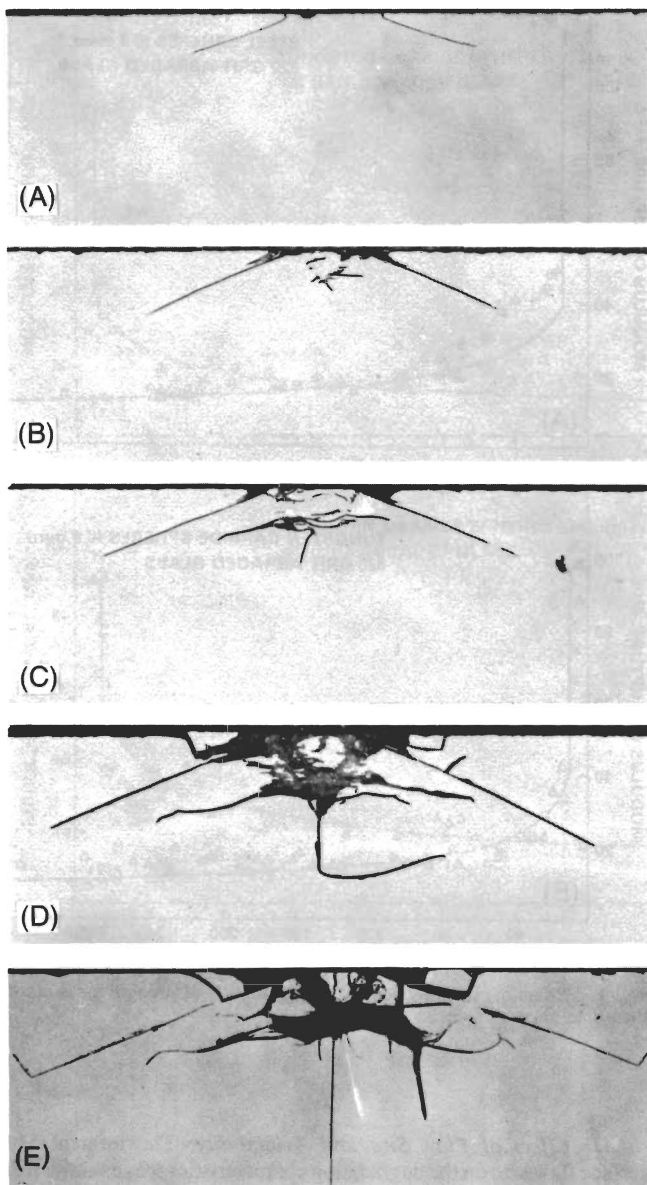


**Fig. 1.** Section-and-etch profiles of damage patterns produced in polished soda-lime glass surfaces by statically loaded WC sphere,  $r=0.5$  mm. Loads were (A) 100 N, (B) 140 N, (C) 180 N, (D) 266 N, and (E) 500 N; width of field in (A)–(D) is 1.5 mm, in (E) 2.5 mm. Note transformation from characteristic “blunt” to “sharp” indenter patterns with increasing load. (From Ref. 11).

was a modified commercial 22-caliber pistol with the gas chamber adapted to operate from tank nitrogen in the gage pressure range 0.35 to 14 MPa. The spheres, of hardened steel or tungsten carbide, were carried by foam plastic sabots; a metal stop at the end of the pistol permitted unrestricted passage of the spheres but prevented the sabots from leaving the barrel. With this modification the pistol was capable of accelerating spheres with a radius of  $\leq 0.8$  mm to velocities of 2 to 300  $\text{m s}^{-1}$ .

The velocity analyzer, based on the time-of-flight principle, was composed of two electromagnetic detectors spaced 150 mm apart and aligned coaxially with the pistol. Each detector consisted of two electromagnetic coils, an excitation coil and a detection coil. The excitation coil had a constant dc current flowing through it to create a magnetic field, which was sensed by the detection coil. Passing through the system, a metallic sphere would perturb this magnetic field, inducing an electric potential in the detection coil. The field perturbations for each detector were recorded as pulses on the time base of a memory oscilloscope. Velocity determinations by this technique were estimated to be accurate to better than 5%.

Target specimens used were glass laths  $\approx 250$  by 37.5 by 5.65 mm.<sup>3,4</sup> Strength was measured in 4-point bending with a major span of 204 mm and a minor span of 37.5 mm, with the impacted face on the tension side. Prior to impactation, most specimens were abraded by a grit-blast treatment with SiC powder over a small central target area, although some were impacted in the as-received state. At low particle velocities ( $\leq 20 \text{ m s}^{-1}$ ), it was necessary first to acid-polish the laths to remove serious edge flaws that might result in premature failure from a source outside the target area. However, some edge failures did occur, and these were omitted from the data accumulation. Immediately after the impact event, the contact site was covered by a drop of mineral oil to minimize any kinetic effects of moisture-assisted crack growth in the subsequent strength test. The delay between impacting the glass laths and measuring their strength never exceeded 4 h.

## (2) Damage Morphology

As the experiments proceeded, it became increasingly apparent that the impact damage patterns were more complex than described in Section II. Although Hertzian cones did invariably form above the threshold impact, they were usually accompanied by secondary cracking more typical of sharp indenters plus a general crushing of the glass in the impact area. Even when cone cracks alone formed during impact, some variants in the morphology were evident.

The nature of the damage was determined by the impact parameters of the impinging sphere and the initial condition of the glass surface. The mechanism for producing the variation in fracture pattern is associated with a tendency for small, hard spheres to penetrate the specimen surface at more severe impact, and thus to behave as sharp indenters. This variability and complexity of morphology made it difficult to obtain representative microphotographs of the entire range of patterns observed. However, the main features were similar to those noted by Phillips<sup>11</sup> in comparative static loading experiments where the control over contact conditions was much greater; a section-and-etch sequence from Phillips' work on polished glass, showing the transition from blunt-indenter to sharp-indenter pattern with increasing penetration, is reproduced here in Fig. 1. In the present experiments, the observations could be most readily reconciled with Fig. 1 by distinguishing three regions of indenter penetrability, allowing for the effects of initial surface condition:

(1) At low penetrations, the indenter produces well-defined cone cracks. If the expanding contact circle encompasses the surface trace of the first crack, then successive ring cracks run downward into the main cone, sometimes forming a detachable collar (Figs. 1 (A) and (B)). The threshold velocity for cone formation in impact was typically 10 to 20  $\text{m s}^{-1}$  on abraded surfaces and somewhat greater, with considerably more scatter, on as-received surfaces.

(2) At intermediate penetrations, median cracks initiate, ultimately growing as half-penny cracks centered on the origin of the contact circle and leaving radial surface traces emanating from the impact zone.<sup>12,13</sup> Figures 1 (C) and (D) show profile views of such cracks starting downward from a subsurface deformation zone. The incidence of median cracking was even more strongly affected by surface preparation than that of cone cracking; although radial traces rarely appeared on surfaces impacted at velocities below  $\approx 30 \text{ m s}^{-1}$  on as-received surfaces, they were prevalent as low as velocities approaching threshold on abraded surfaces. This tendency was noticeably increased with the use of coarser abrasive grits (e.g. 320 mesh to 100 mesh SiC), or spheres of greater density (e.g. steel to tungsten carbide) or smaller radius. In extreme cases, the radial cracks were dominant at all velocities. Generally, both crack types were irregular in appearance; cones tended to be incompletely formed, and medians showed grossly asymmetrical surface traces.

(3) At high penetrations, the damage pattern becomes relatively independent of surface and indenter characteristics. This regime corresponds to velocities above  $\approx 50$  to 100  $\text{m s}^{-1}$ . Although cone and median cracks show comparable dimensions, it is the median cracks which now provide the main source of degradation, since they extend deeper into the plate and normal to the plate surface. Also, at this stage, rapid unloading of the glass surface causes the Hertzian cracks to bend back abruptly toward this surface.<sup>14,15</sup> The network of lateral and other interconnecting cracks which constitute

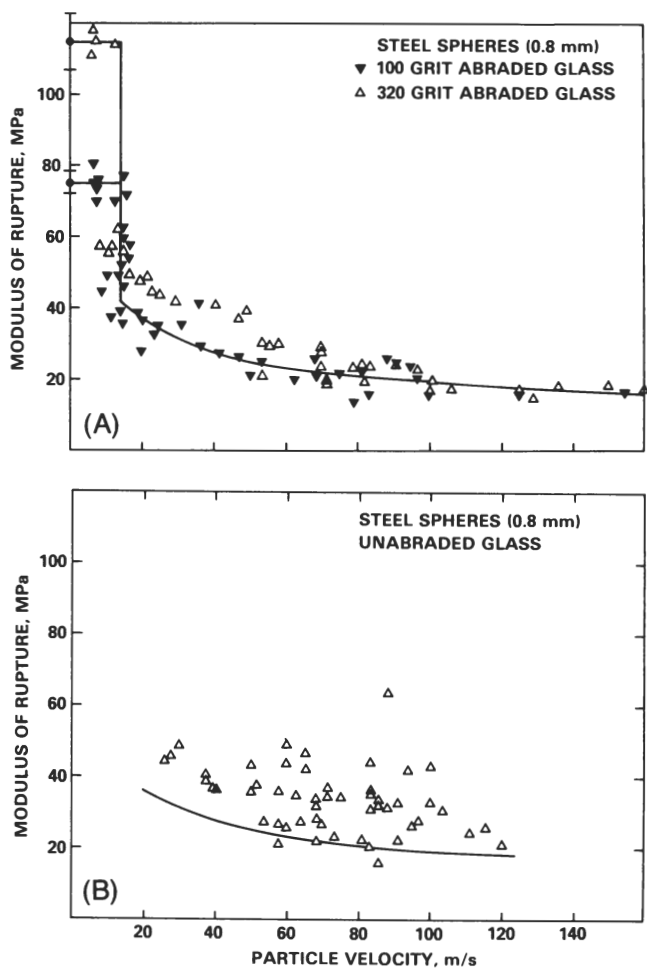


Fig. 2. Strength of soda-lime glass surfaces as function of impact velocity, showing effect of target surface preparation on degradation. Here and in Figs. 3 and 4, data points for unimpacted surfaces at zero velocity represent mean  $\pm$  standard deviation for 10 tests on unimpacted surfaces; solid curves are theoretical predictions from Eqs. (3) and (7); and crosshead speed for bend tests was 50 mm min<sup>-1</sup>, with dominant flaw in oil environment.

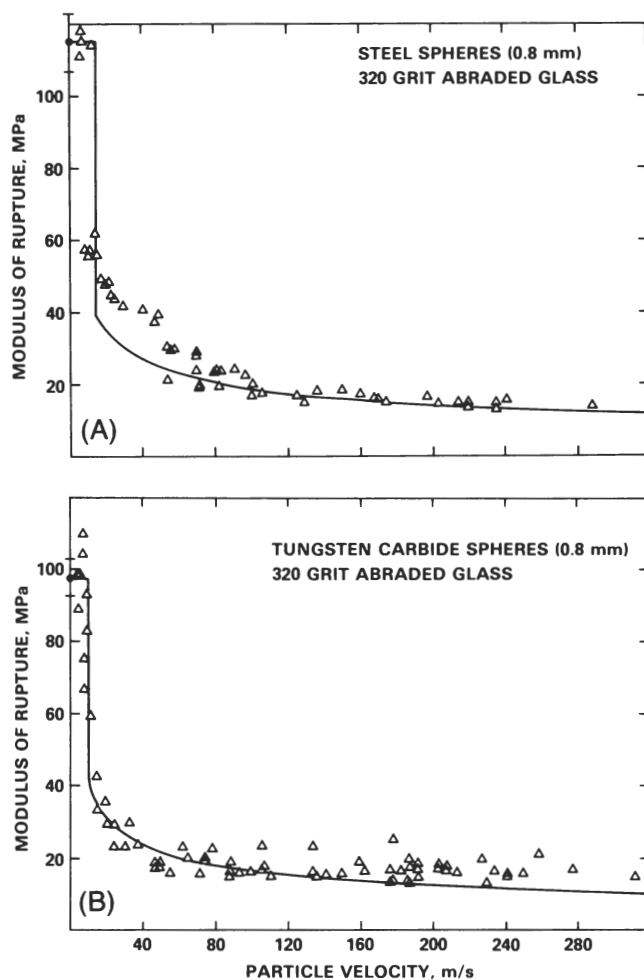


Fig. 3. Effect of projectile density on degradation of strength for abraded soda-lime glass surfaces.

the crushed zone also generates on unloading. All these features are shown in Fig. 1(E). In severe impacts, e.g. 0.8 mm radius tungsten carbide spheres at velocities  $>200$  m s<sup>-1</sup>, the median cracks may actually be driven completely through the glass plates.

### (3) Strength Measurements

To investigate the main features of the theory presented in Section II, we made several series of strength tests as a function of sphere velocity. The test parameters were initial flaw size and sphere density and radius. For each series an appropriate theoretical function  $\sigma(v)$  was evaluated from Eqs. (7) and (3) for comparison with experiment, using the following values: target material constants,<sup>16</sup>  $K_{IC} = (0.70 \pm 0.05)$  MPa m<sup>1/2</sup>,  $E = 70$  GPa and  $\nu = 0.25$  (soda-lime glass); projectile material constants,  $\rho = 7.86 \times 10^3$  kg m<sup>-3</sup> (steel) or  $14.1 \times 10^3$  kg m<sup>-3</sup> (WC); equilibrium indentation fracture constants,<sup>3,5</sup>  $k = 0.66$  (steel/glass) or  $0.55$  (WC/glass),  $\Omega = 0.25 \pm 0.02$  (for cone angle appropriate to soda-lime glass),  $\phi_1^*(\nu) = \phi^*(\nu)(1 - \nu^2) = (1.6 \pm 0.2) \times 10^{-5}$  and  $\beta_R = 28 \pm 2$  (soda-lime glass). The results of the strength degradation analyses are shown in Figs. 2–4, data points representing experiment and solid lines representing theory. Basically, the trends in the degradation curves are the same as observed on statically indented specimens<sup>3</sup>: (1) a low-velocity region of undetectable strength loss, in which surface flaws undergo little or no extension during the impact; (2) a critical-velocity point at which the strength decreases abruptly, corresponding to “pop-in” of an indentation crack; (3) a high-velocity region of slow, steady decline in strength, in which the impact-induced cracks are driven further below the target surface.

(A) *Effect of Flaw Size and Availability:* The influence of surface flaw size on the degradation characteristics was examined in the first tests. Target areas with uniform distributions of 23  $\mu$ m and 10  $\mu$ m flaws, respectively, were prepared by pre-abrasion treatments with 100-grit and 320-grit SiC.<sup>3</sup> Figure 2 (A) shows the results for tests using 0.8-mm-radius steel spheres on glass specimens prepared in this way. As expected (Eq. (7a)), at subcritical velocities the strength holds constant at two separate levels, with the higher strengths corresponding to the finer (320-grit) SiC abrasive. However, the  $v_c$  at which abrupt strength decrease occurs is independent of the surface treatment (as far as can be ascertained within the limits of scatter); this is consistent with the impact version of Auerbach’s law, Eq. (3), in which flaw size does not appear as an independent variable. Finally, at higher velocities the data for both types of specimen approach, and ultimately scatter about, the predicted curve; however, at velocities just above critical, the two sets of data show a small, but systematic, separation, contrary to the absence of any flaw parameters in Eq. (7b). This trend correlates with the observed tendency for median cracks to supplant cone cracks as the main source of degradation with coarser abrasive treatments. For the steel spheres used in Fig. 2, median cracks were dominant at velocities as low as  $\approx 60$  m s<sup>-1</sup> on the 320-grit surfaces and  $\approx 15$  m s<sup>-1</sup> (threshold) on the 100-grit surfaces. Thus the greatest deviations from prediction in Fig. 2(A) actually occur on those surfaces for which the assumption of ideal Hertzian cone fracture is most closely realized.

The derivation of the degradation Eqs. (7) and (3) in Section II is based on the implicit assumption that the glass surface contains an abundance of preexisting cracks which act as nuclei for the prospective indentation fracture process. Controlled abrasion treatments

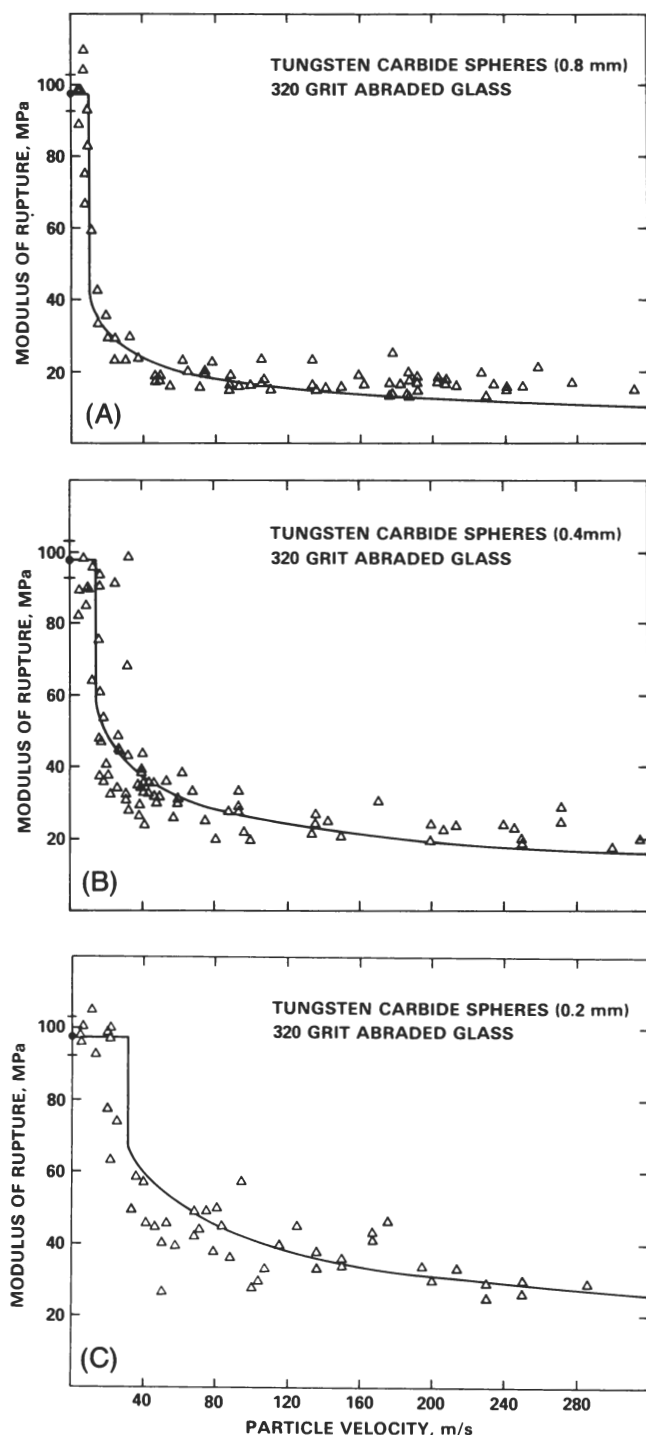


Fig. 4. Effect of projectile radius on degradation of strength for abraded soda-lime glass surfaces.

ensure that this assumption is satisfied, by providing a high density and uniform distribution of surface cracks.<sup>8</sup> Where this precaution is not taken, we have the results for as-received glass surfaces shown in Fig. 2(B). Most of the strength data fall well above the predicted curve, with considerable scatter; this finding is consistent with the observed scatter in threshold velocity. Many of the unabraded target surfaces tested, although ostensibly in the velocity range of strong degradation, showed no sign of impact damage; furthermore, cracks that did form often appeared to be smaller than corresponding cracks in abraded surfaces. This behavior is explained by the scarcity of suitable nucleating flaws in the contact zone.<sup>8</sup> However, it should be emphasized that a single favorably located flaw can cause the strength to decrease to the level characteristic of a surface saturated

with nuclei. Thus, to measure the maximum possible degradation with a minimum of scatter, all subsequent experiments in this work were performed on abraded surfaces.

(B) *Effect of Sphere Density:* The effect of projectile density on strength degradation was checked by comparing data obtained with steel and tungsten carbide spheres of the same size, on glass surfaces subjected to the same abrasion treatment (Fig. 3). These two projectile materials represent a density ratio  $\rho(\text{WC})/\rho(\text{steel}) = 1.81$  and an indentation parameter ratio  $k(\text{WC/glass})/k(\text{steel/glass}) = 0.83$ . At low velocities, the nature of the projectile is irrelevant (any variations in the data being due to nonreproducibilities in the abrasion treatment) (Eq. (7a)). However, since  $v_c \propto k^{7/6} \rho^{-1/2}$  in Eq. (3),  $v_c$  is expected to change in the ratio  $v_c(\text{WC/glass})/v_c(\text{steel/glass}) = 0.60$ ; this appears to be consistent with the depressed value of  $v_c$  in going from the steel to the WC data in Fig. 3. Above  $v_c$  the actual strength value is predicted in Eq. (7b) to vary as  $\sigma \propto \rho^{1/5}$ , i.e.  $\sigma(\text{WC})/\sigma(\text{steel}) = 0.89$ ; the scatter in data in Fig. 3 is apparently too great for any statistically meaningful conclusion to be drawn concerning an effect of this small magnitude. However, a closer scrutiny of the data does reveal a significant difference in agreement between theoretical and experimental results at velocities just above or around critical, with the WC data showing relatively enhanced degradation. This difference also correlates with a greater incidence of median cracking, associated with the enhanced penetration of the denser projectile.

(C) *Effect of Sphere Radius:* Finally, the effect of projectile size on degradation was investigated for tungsten carbide spheres, on glass subjected to a standard abrasion treatment (Fig. 4). While the general trends remain as before, it is clear that the smaller spheres are less deleterious to strength. The  $v_c$  in Eq. (3) varies as  $v_c \propto r^{-5/6}$ , so that we predict an increase in  $v_c$  by a factor of 1.65 each time the sphere radius is halved. Also, since the strength above threshold varies as  $\sigma \propto r^{-2/3}$  in Eq. (7b), we predict a corresponding increase in  $\sigma$  by a factor of 1.59. Both these trends are evident in Fig. 4. Again there is an enhanced penetration effect evident in the data at velocities near critical, with the predominance of median cracking for smaller spheres leading to a strength loss somewhat in excess of that predicted.

#### IV. Discussion

##### (1) Advantages and Implications of the Model

The Hertzian-based model (Section II) provides the foundation for predetermining impact strength-loss characteristics for a given blunt-projectile/brittle-target system. Representing a simple extension of the earlier theory for statically loaded indenters,<sup>3</sup> the present model offers the attractive prospect of designing for strength in terms of readily obtainable indentation fracture constants. All the important parameters appear in simple power form in the degradation Eqs. (7) and (3). This is particularly useful for materials selection, since an optimum combination of fracture mechanics properties, e.g. toughness, stiffness, etc., may be assessed for a given impact situation.

The results also have interesting implications for target surface flaw characteristics and projectile size. First, the degradation curves are relatively insensitive to the size of preexisting flaws (Fig. 2); reducing the surface density of such flaws (for example, going from preabraded to as-received surfaces), increases the average but not the minimum strength at any given impact velocity. Consequently, any attempt to reduce strength loss by removing surface flaws, e.g. by etching, will meet with limited, and uncertain, success; a single spurious flaw can cause maximum degradation. Further, in a case of high projectile penetration, the contact process may produce its own flaws in the target surface (see below). Introducing residual compressive stresses into the target surface seems to be a more practical method for improved degradation resistance.<sup>17</sup>

Secondly, degradation increases with sphere density and radius (Section III). The projectile size effect is important, in that it is opposite to that observed in the corresponding static tests.<sup>3</sup> Thus, although in static loading a larger sphere radius actually produces a lower degradation (the threshold load increasing according to Auerbach's law, Eq. (2), and the subsequent strength-improving cone

crack remaining unaffected in dimension, Eq. (4)), a reverse trend is seen in impact loading because of the counteracting, dominating influence of the magnified impulse, Eq. (1) (both the threshold velocity, Eq. (3), and subsequent strength loss, Eq. (7b), now diminishing). Therefore, the most detrimental particles are those that are large and dense.

## (2) Limitations and Possible Modifications of the Model

In drawing these conclusions, we must remember the discrepancies noted between theory and experiment in Section III. Although these discrepancies seem minor, they are not insignificant, and, for reliability in design, it is essential that we understand their underlying causes. Therefore, we shall concentrate on the mechanisms responsible for the incursion of median cracking in an ostensibly blunt-indenter system and on the conditions under which the quasi-static approach might be expected to break down.

As indicated earlier, in static loading,<sup>12</sup> median cracks are the characteristic fracture mode beneath a penetrating sharp indenter. In well-prepared test surfaces relatively free from flaws, the nuclei for such cracks are found to be deformation-induced within or near the plastic impression zone. Therefore, the hardness of the test material becomes a part of the fracture problem.<sup>12,18</sup> The median cracks observed here with blunt indenters in the limit of high penetration have essentially the same geometry; therefore, we again seek an explanation for their occurrence in terms of a plasticity mechanism.

Suppose that a sphere is loaded onto a specimen surface at increasing elastic contact. In considering the onset of inelastic processes it is helpful to know the relative magnitudes of the various components of the inhomogeneous Hertzian field.<sup>7</sup> For a material with  $\nu=0.25$  we have, in terms of the mean indentation pressure  $p_0 = P/\pi a^2$ , with  $a = (4kPr/3E)^{1/3}$  the contact radius: (1) a primary maximum in the tensile stress,  $0.25 p_0$ , at the contact circle, near where cone cracks initiate, and a secondary maximum,  $0.015 p_0$ , at a depth  $\approx 2a$  below the contact center, near where median cracks initiate; (2) a maximum in the shear stress,  $0.46 p_0$ , at a depth  $\approx 0.5a$  below the contact center, where plasticity processes would be expected to operate; (3) a maximum in the hydrostatic compression,  $1.25 p_0$ , at the contact center itself, where densification processes would be expected to operate.

Referring to the sequence of cross sections for soda-lime glass (Fig. 1), we see in Fig. 1(B) the first appearance of a subsurface deformation zone near the region of the maximum shear stress. Hertzian tests on two crystalline, relatively ductile solids, mild steel<sup>19</sup> and lithium fluoride,<sup>20</sup> have shown that subsurface plasticity sources can operate within the constraint of surrounding elastic material. More recently, Swain and Hagan,<sup>21</sup> by indenting highly polished surfaces with small spheres (0.2 mm radius) to suppress the incidence of cone fracture, were able to make systematic measurements of the same process in alkali silicate glasses. They found that the indentation pressure increased reversibly with contact radius in accordance with the Hertzian equations up to  $p_0 \approx 5$  GPa; beyond this level the pressure saturated, and a permanent set appeared. This value is near the equivalent pressure beneath a standard diamond pyramid indenter, i.e. the Vickers hardness, and may confidently be associated with the same deformation process responsible for hardness impressions. In the present experiments, we may combine the above expressions for  $p_0$  and  $a$  with Eq. (1) to estimate the velocity,  $v_p$ , needed to achieve this plastic yield level: using the constants quoted in Section III(3), we calculate  $v_p \approx 18$  m s<sup>-1</sup> for WC spheres on glass, independent of the sphere radius. This value lies below the threshold velocity,  $v_c \approx 31$  m s<sup>-1</sup>, computed for cone formation in the extreme case of 0.2-mm-radius spheres (Fig. 4(C)).

When the plasticity mechanisms are operating, the sphere penetrates the specimen surface and behaves as a sharp indenter. Swain and Hagan<sup>21</sup> established this penetration as a precursor stage to the generation of median cracks. Similar deformation-induced cracks have been noted by others in ball indentation tests on a range of crystalline materials<sup>22</sup> and plastics.<sup>23</sup> In many of the softer materials the traditional cone fracture was completely absent under all loading conditions. However, the detailed mechanics on median-crack initiation remain obscure, and the estimates of the velocity terms  $v_p$  and  $v_c$  are our only guide to the likely dominance of either

plasticity-induced median cracking or cone cracking. Although in our example above we chose to compare these velocity terms for the most penetrant of the spheres used in the present studies, the values obtained nevertheless indicate a general need to consider plasticity (or, in the case of more open glass structures such as fused silica, densification<sup>24</sup>) processes in the damage evolution.

The observation in Section III(3)(A) that the dominance of median over cone cracking is enhanced by coarser grit preparation of the target surface is still unexplained. It appears that preexisting surface flaws, if sufficiently deep, may actually provide preferential sources for the median cracks. In their ball-indentation study of several crystalline materials, Evans and Wilshaw<sup>22</sup> came to a similar conclusion: they reported the pronounced development of a radial wing-like crack system ("radial" cracks), ultimately developing into the median configuration, on surfaces with machined finishes. The mechanics of initiation in these cases, including the role of local stress concentrations caused by surface roughness effects, is as obscure as in the plasticity mode. While such extraneous sources may be significant in promoting the onset of median cracking, they may be regarded as secondary since the alternative plasticity mechanism is intrinsic and therefore inevitable in the more severe contact situations, i.e. surface sources, although sufficient to initiate the fracture, are not necessary.

Whatever their origin, once median cracks have developed they become the dominant source of strength loss as the impact velocity increases. This transition occurs because cones and medians develop ultimately to comparable dimensions, both assuming an essentially penny-like geometry in their well-developed states of which Eq. (4) is representative ( $R$  now assuming the status of a characteristic crack dimension).<sup>13</sup> However, because of the relative orientation of the two crack types with respect to the tensile field in subsequent plate flexure, the appropriate angular functions for substitution into the degradation Eq. (7) are  $\Omega \approx 0.25$  for cones<sup>3</sup> and  $\Omega \approx 0.4$  for medians.<sup>4</sup> Consequently, since  $\sigma \propto \Omega^{-1/2}$  in Eq. (7b), we might anticipate a depression in the degradation curve of as much as 30% as median cracks begin to take over as the source of dominant flaws. Such an effect is approached in the worst-case situation of Fig. 4(C). However, since several median cracks will usually propagate concurrently with the cone crack, interaction and energy-absorbing mechanisms will reduce the effective  $\Omega$  term,<sup>1-3</sup> particularly at higher velocities. Although not rigorous, arguments of this kind are useful in providing some indication of the limits of reliability of the simple Hertzian model.

The plasticity process referred to above is also pertinent to the spurious cracking (including the upward turn of the Hertzian cones) which is responsible for chipping and crushing at the higher impact velocities. These secondary fracture effects are due primarily to residual stresses generated by stress/strain incompatibility at the elastic/plastic boundary as the sphere unloads from the surface.<sup>12,15</sup> Since the chipping and crushing modes do not produce dominant flaws, they are unlikely to have any direct influence on the strength loss, other than a minor, negative one in absorbing some of the impact energy, but they will contribute substantially to the surface erosion properties. In addition, these same residual stresses may cause further extension of the median cracks, although static loading evidence indicates that no such extension occurs in the direction of the plate thickness.<sup>13</sup>

Thus far we have based our discussion on essentially quasi-static arguments. We have alluded to the existence of certain differences in the damage morphology produced in static and impact loading. High-speed photographic studies of the contact between spherical particles and glass plates show that the impact crack pattern does have the same general features as those seen in Fig. 1.<sup>21,25</sup> The relative enhancement of the median and other secondary cracking at the expense of cone cracking marks the major visual effect of increased load rate. The most likely cause of this effect appears to be a stress reversal on elastic rebound. To effect the rebound the target/projectile interface must accelerate outward beyond the original plane of the glass surface, thereby basically transforming the stress state of the immediate subsurface contact zone from high compression to high tension. The deformation processes originate in this region, which explains the proliferation of the secondary cracking in the impact patterns.

Also evident in the crack morphology is a second dynamic effect, arising from the small contact times in impact situations, typically  $\approx 1 \mu\text{s}$  for the spheres and impact velocities used in the present study.<sup>7</sup> The total time available for cracks to generate and grow will be considerably less than this value because it is necessary for the loading first to achieve threshold and then to build up the driving force to maintain terminal velocity. Thus, for silicate glasses, with terminal velocities  $\approx 1.5 \text{ km s}^{-1}$ ,<sup>26</sup> the maximum extension would be estimated at substantially  $< 1 \text{ mm}$ , a dimension comparable with the scale of cracking in the present tests. In unfavorable cases, we must expect some dynamic limitation in crack growth, especially at the higher impact velocities. This correlates with the observed tendency for cone cracks to form incomplete surface traces and for median crack traces to take on an irregular appearance (Section III(2)). Consequently, we have another factor contributing to the tendency for strength data to lie above the predicted degradation curves at high velocities.

Of course, a true dynamic analysis of particle impact is much more complex than we have intimated here. The changing nature of the elastic/plastic indentation field as the incident velocity approaches sonic levels, ensuing stress-wave effects, etc., constitute an important regime beyond the scope of this work: this area is currently receiving attention elsewhere.<sup>27-29</sup>

Additional secondary factors in the crack morphology are interfacial contact friction and surface roughness. Friction between projectile and target tends to inhibit cone formation during the loading half-cycle, but to promote multiple cracking on unloading.<sup>30</sup> However, once the crack is fully developed, it is unlikely to be influenced by frictional tractions at the contact, since these, according to St. Venant's principle,<sup>7</sup> tend rapidly to a zero net driving force at the crack front. Similarly, we expect surface roughness effects to be localized at the contact area; thus they have little influence on ultimate crack propagation. However, since both friction and roughness must modify the local subsurface stress distribution where irreversible processes occur, they might be expected to play some role in the contest between cone and median crack initiation.

Several sources of discrepancy in the simple Hertzian fracture model have been discussed at some length. Of these sources, those responsible for the formation of median cracks (notably plasticity mechanisms) are of greatest concern, for when only Hertzian cracks are formed the strength data tend always to lie above the predicted degradation curve. Thus the theory serves as a useful basis for safe design, except in extreme cases where the spherical impactor begins to penetrate the surface. In such extreme cases the distinction between "blunt" and "sharp" indenters is no longer well defined. An ultraconservative approach would then involve the use of sharp-indenter theory<sup>4</sup> to provide a lower bound to the strength characteristics over the entire range of impact conditions; as already indicated, an effective first step in this direction would be a simple modification of the angular function  $\Omega$  in Eq. (7). However, for a truly pointed indenter it would also be necessary to reexamine the basic starting assumptions under which the indentation loading is determined from the impact velocity; that is, Eq. (1) would need to be rederived in terms of a completely different set of contact conditions. A study of strength degradation in sharp-particle impact is currently under way in these laboratories.

## V. Conclusions

A theory of strength degradation, based on quasi-static Hertzian fracture mechanics, has been developed for brittle targets impacted with spherical projectiles. The basic analysis in Section II makes no explicit assumptions about the nature of the impacting materials, other than that the projectile material be elastic and the target material be elastic/brittle: thus, while the present study has dealt specifically with soda-lime glass targets, the theory might be applied to other ceramic materials with the same degree of confidence or reservation. In designing with a material whose conventional fracture mechanics properties are well documented, it is necessary only to predetermine 2 adjustable constants ( $\phi_1^*$  and  $\beta_R$ ) in Eqs. (7) and (3) by routine indentation-fracture testing.

Results of this study are summarized as follows:

(1) For a given projectile/target system the Hertzian-based strength/velocity degradation curve shows three distinct regions (Figs. 2 through 4): at low impact velocities ( $v < v_c$ , Eq. (7a)), zero (or undetectable) strength loss, indicating negligible growth of flaws in the target surface; at threshold velocity ( $v = v_c$ , Eq. (3)), a reasonably well-defined, abrupt strength decrease, corresponding to pop-in of a cone crack; at high velocities ( $v > v_c$ , Eq. (7b)), a steady strength decline with velocity, corresponding to stable growth of the cone crack.

(2) The more hostile mechanical environments, as quantified by a lower value of  $v_c$  in Eq. (3) or strength in Eq. (7), are those for which the impacting particles are dense ( $v_c \propto \rho^{1/2}$ ,  $\sigma(v > v_c) \propto \rho^{-1/5}$  (Fig. 3)) or large ( $v_c \propto r^{-5/6}$ ,  $\sigma(v > v_c) \propto r^{-2/3}$  (Fig. 4)).

(3) The target materials with greatest resistance to degradation are those with high toughness ( $\sigma(v < v_c) \propto K_{Ic}$ ,  $v_c \propto K_{Ic}^{5/3}$ ,  $\sigma(v > v_c) \propto K_{Ic}^{4/3}$ ). (Elastic stiffness also enters, via the  $k/E$  term in Eqs. (3) and (7), but is less easily evaluated because of its involvement in the  $K_{Ic}$  term, Eq. (2).) Flaw parameters are relatively unimportant, entering explicitly only in the low-velocity strength, Eq. (7a) ( $\sigma(v < v_c) \propto c_f^{0-1/2}$  (Fig. 2)); thus surface preparation is not a factor in the strength characteristics at severe impact.

(4) The experimental strength data show some deviation from the idealized Hertzian-based theory. Whenever only cone cracks are formed, the data points lie above the computed curve, in which case the predictions are conservative. However, when cone cracking is supplanted by median cracking, the data points may fall below the computed curve and predictions are no longer conservative. By considering the relative orientation of the two types of cracks, we can anticipate a depression in the degradation curve of as much as 30%, as median cracks take over as the source of dominant flaws. Therefore, by modifying the theory to account for median crack formation, a conservative theory for predicting strength degradation may be obtained. Median crack formation is attributed to subsurface plasticity processes, accentuated by using spheres of higher density and smaller radius (notably in Fig. 4(C)) and, to a lesser extent, to more severe starting flaws (Fig. 2). The deleterious effect of median cracking on strength is largely counteracted at higher velocities by the opposite effects of factors such as multiple cracking and dynamic limitations on crack extension.

**Acknowledgments:** The authors are grateful to H. H. Johnson, D. E. Roberts, P. Serber, and S. Parkes for assistance with the experiments; to M. V. Swain for providing access to unpublished work; to K. Phillips for providing Fig. 1; and to A. G. Evans for discussions.

## References

- R. D. Southwick and R. E. Mould, results reported by R. E. Mould; pp. 119-49 in *Fracture of Metals, Polymers and Glasses (Fundamental Phenomena in the Materials Sciences, Vol. 4)*, Edited by L. J. Bonis, J. J. Duga, and J. J. Gilman. Plenum, New York, 1967.
- J. P. Ashford; pp. 173-89 in *Special Ceramics 4*, Edited by P. Popper. British Ceramic Research Association, Stoke-on-Trent, England, 1968.
- B. R. Lawn, S. M. Wiederhorn, and H. H. Johnson, "Strength Degradation of Brittle Surfaces: Blunt Indenters," *J. Am. Ceram. Soc.*, **58** [9-10] 428-32 (1975).
- B. R. Lawn, E. R. Fuller, and S. M. Wiederhorn, "Strength Degradation of Brittle Surfaces: Sharp Indenters," *ibid.*, **59** [5-6] 193-97 (1976).
- B. R. Lawn and T. R. Wilshaw, "Indentation Fracture: Principles and Applications," *J. Mater. Sci.*, **10** [6] 1049-81 (1975).
- A. G. Evans, "Strength Degradation by Projectile Impacts," *J. Am. Ceram. Soc.*, **56** [8] 405-409 (1973).
- S. Timoshenko and J. N. Goodier, *Theory of Elasticity*, 2d ed.; pp. 372-84. McGraw-Hill, New York, 1951.
- F. B. Langitan and B. R. Lawn, "Hertzian Fracture Experiments on Abraded Glass Surfaces as Definitive Evidence for an Energy Balance Explanation of Auerbach's Law," *J. Appl. Phys.*, **40** [10] 4009-17 (1969).
- F. C. Frank and B. R. Lawn, "Theory of Hertzian Fracture," *Proc. R. Soc. London, Ser. A*, **299** [1458] 291-306 (1967).
- F. C. Roesler, "Brittle Fractures Near Equilibrium," *Proc. R. Soc. London, Ser. B*, **69** [10] 981-92 (1956).
- K. Phillips, "Study of the Free Abrasive Grinding of Glass and Fused Silica"; Ph.D. Thesis, University of Sussex, England, 1975; also in Fig. 21 of Ref. 5.
- B. R. Lawn and M. V. Swain, "Microfracture Beneath Point Indentations in Brittle Solids," *J. Mater. Sci.*, **10** [1] 113-22 (1975).
- B. R. Lawn and E. R. Fuller, "Equilibrium Penny-Like Cracks in Indentation Fracture," *ibid.*, [12] 2016-2024.
- C. J. Culf, "Fracture of Glass Under Various Liquids and Gases," *J. Soc. Glass Technol.*, **41** [199] 157-67T (1957).
- B. R. Lawn, M. V. Swain, and K. Phillips, "Mode of Chipping Fracture in Brittle Solids," *J. Mater. Sci.*, **10** [7] 1236-39 (1975).
- S. M. Wiederhorn, "Fracture Surface Energy of Glass," *J. Am. Ceram. Soc.*, **52** [2] 99-105 (1969).

- <sup>17</sup> D. B. Marshall and B. R. Lawn, "Strength Degradation of Thermally Tempered Glass Plates"; to be published in the *Journal of the American Ceramic Society*.
- <sup>18</sup> A. G. Evans and E. A. Charles, "Fracture Toughness Determinations by Indentation," *J. Am. Ceram. Soc.*, **59** [7-8] 371-72 (1976).
- <sup>19</sup> R. M. Davies, "Determination of Static and Dynamic Yield Stresses Using a Steel Ball," *Proc. R. Soc. London, Ser. A*, **197** [1050] 416-32 (1949).
- <sup>20</sup> M. V. Swain and B. R. Lawn, "Study of Dislocation Arrays at Spherical Indentations in LiF as a Function of Indentation Stress and Strain," *Phys. Status Solidi*, **35** [2] 909-23 (1969).
- <sup>21</sup> (a) M. V. Swain and J. T. Hagan, "Indentation Plasticity and Ensuing Fracture of Glass," *J. Phys. D.*, **9**, 2201-14 (1976).
- (b) C. G. Knight, M. V. Swain, and M. M. Chaudhri, "Impact of Small Steel Spheres on Glass Surfaces"; unpublished work.
- <sup>22</sup> A. G. Evans and T. R. Wilshaw, "Quasi-Plastic Solid Particle Damage in Brittle Materials," *Acta Metall.*, **24**, 939-56 (1976).

- <sup>23</sup> K. E. Puttick, L. S. A. Smith, and L. E. Miller, "Stress Fields Around Indentations in Poly (Methyl Methacrylate)"; unpublished work.
- <sup>24</sup> F. M. Ernsberger, "Role of Densification in Deformation of Glasses Under Point Loading," *J. Am. Ceram. Soc.*, **51** [10] 545-47 (1968).
- <sup>25</sup> Frank Kerkhof and H. Mueller-Beck, "Fracture Mechanics Interpretations for Impact Marks on Stone Objects," *Glastech. Ber.*, **42** [10] 439-48 (1969).
- <sup>26</sup> B. R. Lawn and T. R. Wilshaw, *Fracture of Brittle Solids*; Ch. 5. Cambridge University Press, London, 1975.
- <sup>27</sup> W. F. Adler; unpublished work.
- <sup>28</sup> A. G. Evans; unpublished work.
- <sup>29</sup> E. Rockar; unpublished work.
- <sup>30</sup> K. L. Johnson, J. J. O'Connor, and A. C. Woodward, "Effect of the Indenter Elasticity on the Hertzian Fracture of Brittle Materials," *Proc. R. Soc. London, Ser. A*, **334** [1596] 95-117 (1973).